JACS
JOURNAL OF THE AMERICAN CHEMICAL SOCIETY
Article
pubs.acs.org/JACS

Direct Observation by Rapid-Scan FT-IR Spectroscopy of Two-Electron-Reduced Intermediate of Tetraaza Catalyst $[Co^{II}N_4H(MeCN)]^{2+}$ Converting CO_2 to CO

Hua Sheng and Heinz Frei*

Molecular Biophysics and Integrated Bioimaging Division, Lawrence Berkeley National Laboratory, University of California, Berkeley, California 94720, United States

Supporting Information

ABSTRACT: In the search for the two-electron-reduced intermediate of the tetraaza catalyst $[Co^{II}N_4H(MeCN)]^{2+}$ (N_4H = 2,12-dimethyl-3,7,11,17-tetraazabicyclo[11.3.1]-heptadeca-1(17),2,11,13,15-pentaene) for CO_2 reduction and elementary steps that result in the formation of CO product, rapid-scan FT-IR spectroscopy of the visible-light-sensitized catalysis, using $Ir(ppy)_3$ in wet acetonitrile (CD_3CN) solution, led to the observation of two sequential intermediates. The initially formed one-electron-reduced $[Co^{I}N_4H]^{+}-CO_2$ adduct was converted by the second electron to a transient $[Co^{I}N_4H]^{+}-CO_2^{-}$ complex that spontaneously converted CO_2 to CO in a rate-limiting step on the second time scale in the dark under regeneration of the catalyst (room temperature). The macrocycle IR spectra of the $[Co^{I}N_4H]^{+}-CO_2^{-}$ complex and the preceding one-electron $[Co^{I}N_4H]^{+}-CO_2$ intermediate show close similarity but distinct differences in the carboxylate modes, indicating that the second electron resides mainly on the CO_2 ligand. Vibrational assignments are corroborated by ^{13}C isotopic labeling. The structure and stability of the two-electron-reduced intermediate derived from the time-resolved IR study are in good agreement with recent predictions by DFT electronic structure calculations. This is the first observation of an intermediate of a molecular catalyst for CO_2 reduction during the bond-breaking step producing CO. The reaction pathway for the Co tetraaza catalyst uncovered here suggests that the competition between CO_2 reduction and proton reduction of a macrocyclic multi-electron catalyst is steered toward CO_2 activation if the second electron is directly captured by an adduct of CO_2 and the one-electron-reduced catalyst intermediate.

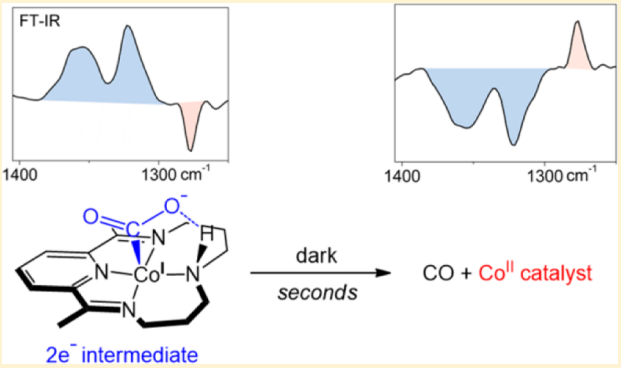

1. INTRODUCTION

Cobalt and nickel heteroaromatic macrocycle complexes are well known for their ability to reduce carbon dioxide to carbon monoxide or formate in aqueous or wet organic solvents in competition with the generation of hydrogen.[1−7] In light of the sparsity of molecular catalysts for CO_2 reduction when compared with the considerable variety of molecular catalysts for H^+ reduction,[8−17] steering the selectivity toward CO_2 conversion at the expense of hydrogen generation with the goal of expanding the pool of carbon dioxide activation catalysts for electrocatalysis or artificial photosynthesis is highly desirable. This requires a detailed understanding of the mechanistic aspects that direct the catalysis from proton reduction toward CO_2 activation.

Intermediates of molecular CO_2 reduction catalysts have been spectroscopically observed under reaction conditions for several organometallic systems. In early work, Fujita and co-workers identified a 5-coordinated Co^{I} tetraazadiene$-CO_2$ complex as one-electron reduction intermediate of visible-light-sensitized CO_2 reduction of the Co^{II} tetraaza catalyst and detected the subsequently formed 6-coordinated solvent$-Co^{III}-CO_2^{2-}$ complex by nanosecond optical absorption spectroscopy.[18] The structure of the as-synthesized Co^{I} complex was determined by FT-IR and NMR spectroscopy. By reducing Ni^{II} tetraaza catalyst by pulse radiolysis, the same group reported more recently UV−vis spectra of a $Ni^{I}-CO_2$ adduct.[2,3] For Co phthalocyanine catalysts, two-electron-reduced species prior to interaction with CO_2 were observed by UV−vis spectroscopy.[19,20] For Re and Mn bipyridyl carbon monoxide type catalysts, Kubiak discovered the CO_2 reduction intermediate Re(*tert*-butyl-bpy)$(CO)_3(COOH(\eta^1))$ of the Re^{I}(4,4′-di-*tert*-butyl-2,2′-bipyridyl)$(CO)_3Cl$ catalyst by stopped-flow/rapid-scan FT-IR spectroscopy,[21] which was preceded by detection of the precursor complex [Re(*tert*-butyl-bpy)-$(CO)_3]^-$ by IR spectroelectrochemistry.[22,23] Inoue subsequently detected the same intermediate for Re(dimethyl-bpy)$(CO)_3Cl$ under photocatalytic reaction conditions by FT-IR as well cold-spray ionization mass spectroscopy.[24] This intermediate forms a Re carboxylate dimer upon insertion of a

Received: May 21, 2016
Published: July 15, 2016

DOI: 10.1021/jacs.6b05248
J. Am. Chem. Soc. 2016, 138, 9959−9967

second CO_2 molecule prior to spontaneous conversion to CO and carbonate-bridged dimer according work by the Brookhaven group.[25,26] The one-electron intermediate or its dimer for related Mn catalysts [Mn^I(di-*tert*-butyl-bpy)-$(CO)_3Br$] and [Mn(dimethyl-bpy)$(CO)_3Br$] were detected by pulse radiolysis coupled with IR laser spectroscopy[27] and pulsed EPR spectroscopy,[28] respectively. Knowledge of these intermediates has greatly advanced the mechanistic understanding of these reactions. However, intermediates spectroscopically identified todate under reaction conditions are still one or more elementary steps short of the bond rearrangement step that converts CO_2 to CO or formate.

In a recent electrochemical study of the macrocycle complex $[Co^{III}\mathbf{N_4H}(Br)_2]^+$ ($\mathbf{N_4H}$ = 2,12-dimethyl-3,7,11,17-tetraazabicyclo[11.3.1]heptadeca-1(17),2,11,13,15-pentaene), Lacy et al. found in CO_2-saturated wet acetonitrile (10 M H_2O) solution a Faradaic efficiency of 45% for CO generation and a CO to H_2 ratio of 3:2 near the $Co^{I/0}$ potential.[29] This is interesting because Co N_4–macrocycle complexes typically favor H^+ over CO_2 reduction.[30,31] In an effort to detect a possible intermediate formed at the $Co^{I/0}$ potential with a structure-specific spectroscopy that might provide mechanistic insight into the competition between the two reaction products, Zhang et al. employed in situ FT-IR spectroscopy and observed a CO_2 adduct of the one-electron $[Co^I\mathbf{N_4H}]^+$ intermediate in wet acetonitrile solution using $[Ru(bpy)_3]^{2+}$ as visible light sensitizer (catalyst complex shown in Figure 1).[32] Interpretation was guided by concurrent electronic structure calculations that predict a weak interaction of the $[Co^I\mathbf{N_4H}]^+$ complex with CO_2.[32] While no CO product was detected in experiments with the Ru sensitizer, use of $Ir(ppy)_3$ sensitizer with sufficient reduction potential to reduce the Co^I catalyst (ε^0 = −1.46 V (SCE)) led to the observation of CO, consistent with the substantially larger reduction potential of the $Ir(ppy)_3$ compared to the $[Ru(bpy)_3]^{2+}$ sensitizer (−1.73 and −1.33 V (vs SCE), respectively). However, a reaction intermediate following transfer of the second electron to the Co catalyst, which is expected to provide critical insight into factors steering the pathway toward CO_2 reduction, has so far escaped detection.

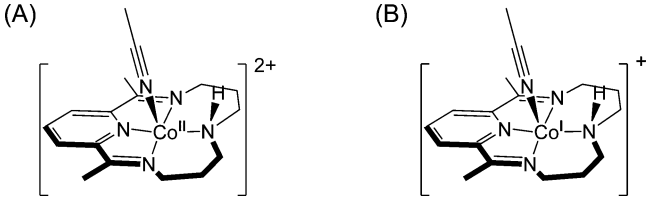

Figure 1. Structure of (A) $[Co^{II}(\mathbf{N_4H})(MeCN)]^{2+}$ and (B) $[Co^I(\mathbf{N_4H})(MeCN)]^+$.

We report here IR detection and monitoring of the kinetics of a two-electron-reduced transient intermediate of CO_2 reduction starting from the $[Co^{II}\mathbf{N_4H}]^{2+}$ resting state in wet acetonitrile solution by rapid-scan FT-IR spectroscopy. Experiments were conducted by visible light photosensitization in a mixture of CD_3CN and H_2O, which allowed us to record large sections of the macrocycle IR spectrum of the one- and two-electron transfer intermediates. This is the first observation of an intermediate of a molecular catalyst for CO_2 reduction during the bond breaking step that produces CO. IR spectroscopy of the preceding one-electron reduction step revealed that the $[Co^I\mathbf{N_4H}]^+$–CO_2 carboxylate intermediate is formed with high selectivity. Based on these observations, mechanistic factors emerge that may lead to preferential CO_2 reduction over proton reduction of macrocycle catalysts.

2. EXPERIMENTAL SECTION

2.1. Chemicals. The catalyst $[Co^{II}\mathbf{N_4H}(MeCN)_2](BPh_4)_2$ and the one-electron-reduced complex $[Co^I\mathbf{N_4H}(MeCN)](BPh_4)$ were synthesized following a previously reported method.[29] While the Co^{II} complex in the solid bis-BPh_4 salt has two acetonitrile ligands, once dissolved in acetonitrile, the complex is 5-coordinated and has just one acetonitrile ligand as shown by UV–vis spectroscopy.[29] $Ru(bpy)_3Cl_2\cdot(H_2O)_6$ (bpy = 2,2′-bipyridine), $Ir(ppy)_3$ (ppy^- = phenylpyridine anion), triethylamine (TEA), acetonitrile-d_3 (99.8 atom % D), and $^{13}CO_2$ (99 atom % ^{13}C, <3 atom % ^{18}O) were purchased from Sigma-Aldrich and used as received.

2.2. Spectroscopy of Photocatalysis. To prepare the sample for FT-IR measurements, 3 mM $[Co^{II}\mathbf{N_4H}(MeCN)_2](BPh_4)_2$, 1 mM $Ru(bpy)_3^{2+}$ (or 0.2 mM $Ir(ppy)_3$) and 50 mM TEA were dissolved in wet CD_3CN (0.1 or 1 M H_2O) followed by bubbling of Ar and $^{12}CO_2$ (or $^{13}CO_2$) gas for a few minutes inside a N_2 glovebox. To minimize the presence of O_2, the resulting solution was sealed in a 200 μm path-length CaF_2 liquid cell in the glovebox.

A FT-IR spectrometer Bruker model Vertex 80 equipped with a HgCdTe PV detector (Kolmar Technologies model KMPV11-1-J2, 14 μm band gap) was used. In the rapid-scan mode, the spectra were recorded in a double-sided/forward–backward mode with the mirror velocity of 160 kHz and spectral resolution of 4 cm^{-1}. The photolysis source for the photocatalytic reaction was a 405 nm diode laser (Spectra Physics, 200 mW max. power). Light pulses were generated by intercepting the laser beam by a mechanical shutter with variable opening times (Vincent Associates model Uniblitz, controlled by a BNC pulse/delay generator model 565). For precise synchronization of photolysis pulse and spectral data acquisition, opening of the shutter was triggered by the forward motion of the interferometer mirror. The sample in the CaF_2 cell was irradiated for 7.2 s, and the FT-IR data were recorded *in situ* both during the irradiation and the following dark period. Samples were discarded after each measurement, and the results of three consecutive experiments were averaged for further signal-to-noise improvement.

3. RESULTS

3.1. Interaction of $[Co^{II}N_4H(MeCN)]^{2+}$ and $[Co^IN_4H(MeCN)]^+$ with CO_2. IR spectra of $[Co^{II}\mathbf{N_4H}(MeCN)]^{2+}$ catalyst complex (5 mM) in wet CD_3CN solution (0.1 M H_2O) after bubbling of CO_2 showed new bands at 1640 ($^{13}CO_2$: 1590 cm^{-1}) and 1674 cm^{-1} ($^{13}CO_2$: 1628 cm^{-1}) originating from HCO_3^- (bicarbonate)[33−35] coordinated to the Co^{II} complex, while all other bands of the catalyst remained unchanged, as shown in Figure 2a,b. No free bicarbonate was observed. For clarity, the IR bands of the CD_3CN, H_2O and the $[B(C_6H_5)_4]^-$ counterion at 1267, 1427, 1481, and 1581 cm^{-1} were subtracted in all spectra shown in this paper using the spectrum of $NaB(C_5H_6)_5$ in CD_3CN as reference (Figure S1). The complete list of the IR bands of the $[Co^{II}\mathbf{N_4H}(MeCN)]^{2+}$ and the $[Co^{II}\mathbf{N_4H}]^{2+}$–$HCO_3^-$ complexes are given in Table 1. While IR absorptions of the sensitizer $[Ru(bpy)_3]^{2+}$ or $Ir(ppy)_3$ were very weak at the low concentration used, the sacrificial donor TEA (triethylamine) readily showed absorptions presented in Figure S1. In the presence of 0.05 M TEA, the $[Co^{II}\mathbf{N_4H}]^{2+}$ catalyst gives rise to additional peaks at 1268 and 1338 cm^{-1}, higher intensity of the 1403 cm^{-1} band, and additional intense bands at 1474, 1590, and 1684 cm^{-1} as shown in Figure 2c and summarized in Table 1, which are attributed to complex formation between TEA and the nucleophilic Co^{II} center of the catalyst. At the

DOI: 10.1021/jacs.6b05248
J. Am. Chem. Soc. 2016, 138, 9959–9967

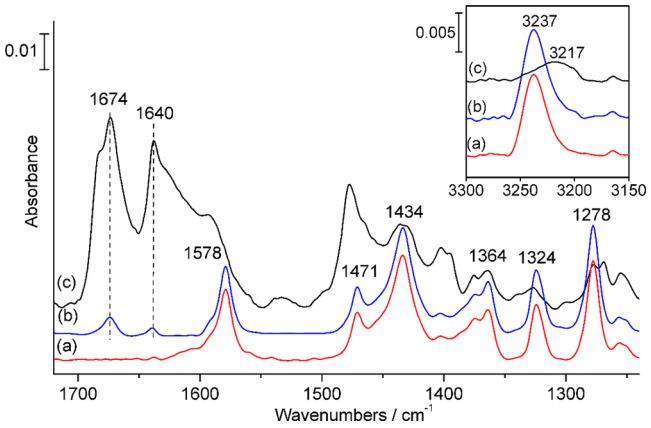

Figure 2. FT-IR spectra of the $[Co^{II}N_4H(MeCN)]^{2+}$ catalyst. (a) $[Co^{II}N_4H(MeCN)]^{2+}$ (5 mM) in CD_3CN containing 0.1 M H_2O. (b) The same solution after bubbling of CO_2. (c) After adding 50 mM TEA and bubbling of CO_2. Inset shows the NH stretch mode of the three samples. In all spectra, bands of solvent CD_3CN, H_2O, and counterion $B(C_6H_5)_4^-$ were subtracted.

Table 1. IR Frequencies of $[Co^{II}N_4H(MeCN)]^{2+}$ in Wet CD_3CN (0.1 M H_2O), When Saturated with $^{12}CO_2$ ($^{13}CO_2$), and in the Presence of TEA

	$[Co^{II}N_4H(MeCN)]^{2+}$ w/CO_2		$[Co^{II}N_4H(MeCN)]^{2+}$ w/CO_2 w/TEA	
$[Co^{II}N_4H(MeCN)]^{2+}$	$^{12}CO_2$	$^{13}CO_2$	$^{12}CO_2$	$^{13}CO_2$
3237	3237		3217	
1578	1674	1628	1674	1628
1471	1640	1590	1684	
1434	1578		1640	1590
1403	1471		1590	
1374	1434		1474	
1364	1403		1434	
1324	1374		1403	
1278	1364		1374	
1256	1324		1364	
	1278		1338	
	1256		1324	
			1278	
			1268	

same time, the bicarbonate absorptions at 1640 and 1674 cm^{-1} are much more intense than in the absence of TEA (corresponding $^{13}CO_2$ spectrum shown in Figure S2). This is due to additional formation of HCO_3^- since TEA acts as a base in the presence of H_2O and CO_2,[25] Small amounts of CO_3^{2-} (carbonate) are also formed as indicated by a weak band at 1529 cm^{-1} (^{13}C: 1491 cm^{-1}).[36,37] The substantial red shift of 20 cm^{-1} of the NH stretch, from 3237 to 3217 cm^{-1} (inset of Figure 2), shows the H bonding interaction between the bicarbonate O and the macrocycle amine group of the $[Co^{II}N_4H]^{2+}$–HCO_3^- complex according to the structure shown in Figure 3.

As-synthesized one-electron-reduced $[Co^{I}N_4H(MeCN)]^+$ catalyst in CD_3CN (0.1 M H_2O) has an IR spectrum shown in Figure 4, trace (a) with frequencies presented in Table 2.

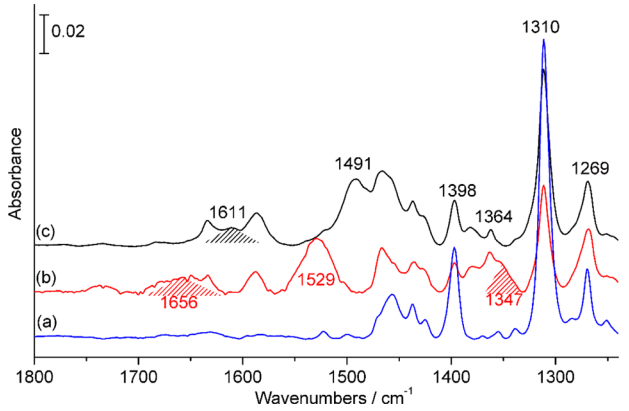

Figure 4. FT-IR spectra of one-electron-reduced catalyst. (a) FT-IR spectrum of $[Co^{I}N_4H(MeCN)]^+$ (5 mM) in CD_3CN containing 0.1 M H_2O. (b) The same solution after bubbling of $^{12}CO_2$. (c) Solution after bubbling of $^{13}CO_2$. In all spectra, bands of solvent CD_3CN, H_2O and counterion $B(C_6H_5)_4^-$ were subtracted.

Table 2. IR Frequencies of $[Co^{I}N_4H(MeCN)]^+$, $[Co^{I}N_4H]^+$–CO_2, and (Two-Electron-Reduced) $[Co^{I}N_4H]^+$–CO_2^- in Wet CD_3CN (0.1 M H_2O)

	$[Co^{I}N_4H]^+$–CO_2		$[Co^{I}N_4H]^+$–CO_2^-	
$[Co^{I}N_4H(MeCN)]^+$	$^{12}CO_2$	$^{13}CO_2$	$^{12}CO_2$	$^{13}CO_2$
3251	3230			
1522	1656	1611	1587	
1500	1635		1466	
1471	1587		1437	
1456	1466		1364	
1437	1437		1356	1310
1425	1364		1324	
1398	1347	1308	1269	
1370	1324		1251	
1355	1269			
1339	1251			
1310				
1269				
1251				

After bubbling CO_2, new bands appeared at 1324, 1347, 1364, 1466, 1587, 1635, and 1656 cm^{-1}(broad) (Figure 4, trace (b)). As shown in trace (c) of Figure 4, in the presence of $^{13}CO_2$ the 1347 cm^{-1} band shifts to 1308 cm^{-1} (overlapped by the 1310 cm^{-1} macrocycle mode). For clarity, the same ^{12}C and ^{13}C spectra but with the bands of $[Co^{I}N_4H(MeCN)]^+$ subtracted are shown in Figure 5B. Frequency and ^{13}C shift of the 1347

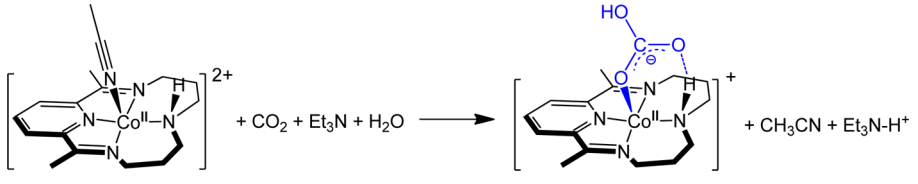

Figure 3. Proposed structure of complex of bicarbonate with $[Co^{II}N_4H]^{2+}$.

DOI: 10.1021/jacs.6b05248
J. Am. Chem. Soc. 2016, 138, 9959–9967

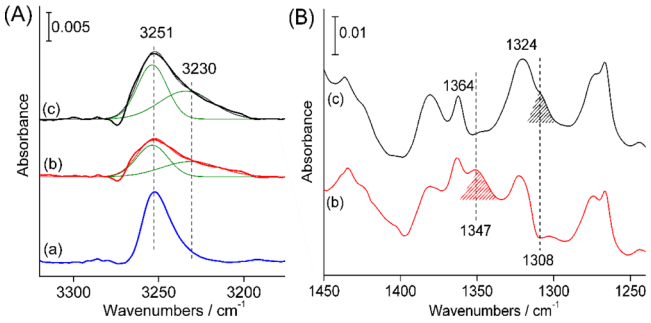

Figure 5. FT-IR spectra of one-electron-reduced catalyst. (A) ν(N−H) region of spectra (a), (b), and (c) of Figure 4. (B) Spectrum (b) of Figure 4 with the bands of $[Co^{I}\mathbf{N_4H}(MeCN)]^+$ species subtracted. (c) Spectrum (c) of Figure 4 with bands of $[Co^{I}\mathbf{N_4H}(MeCN)]^+$ species subtracted. In all spectra, bands of solvent CD_3CN, H_2O, and counterion $B(C_6H_5)_4^-$ were subtracted. Spectral deconvolution on (A) was conducted with Origin software.

cm^{-1} band are consistent with the symmetric stretch of carboxylate that interacts with the Co^I center through carbon, which is confirmed by broad absorption of the asymmetric carboxylate stretch at 1656 cm^{-1} (^{13}C: 1611 cm^{-1}).

Furthermore, in the presence of CO_2 the ν(NH) mode of $[Co^{I}\mathbf{N_4H}(MeCN)]^+$ at 3251 cm^{-1} is accompanied by a band at 3230 cm^{-1} indicating engagement of the amine moiety in H bonding with the carboxylate ligand (Figure 5A), in agreement with prediction by DFT calculations.[32] The formation of a carboxylate complex of CO_2 with the Co^I reflects the nucleophilic property of the reduced Co center. IR stretch modes of CO_2 adducts on Co centers in the formal oxidation state 1+ stabilized by secondary sphere interactions have been reported previously.[38−40] Spectral deconvolution of the NH absorption indicates that approximately half of the reduced catalyst species form a $[Co^{I}\mathbf{N_4H}]^{1+\delta}-CO_2^{\delta-}(\eta^1)$ carboxylate complex as illustrated in Figure 6. The new absorptions at

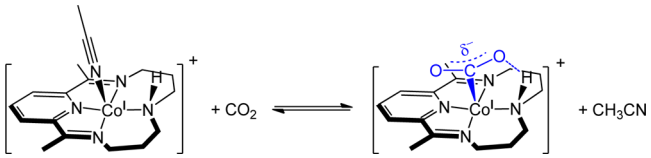

Figure 6. Proposed structure of complex of CO_2 with $[Co^{I}\mathbf{N_4H}]^+$.

1324, 1364, 1466, 1587, and 1635 cm^{-1} point to structural distortion and electron redistribution of the macrocycle as a result of CO_2 coordination. No significant spectral changes of $[Co^{I}\mathbf{N_4H}]^+-CO_2$ or $[Co^{I}\mathbf{N_4H}(MeCN)]^+$ species were observed upon addition of TEA to the solution. IR bands of the various Co^I complexes are summarized in Table 2.

3.2. CO_2 Reduction with $[Ru(bpy)_3]^{2+}$ Sensitizer. Upon illumination of a wet CD_3CN solution (0.1 M H_2O) containing 3 mM $[Co^{II}\mathbf{N_4H}(MeCN)]^{2+}$, 1 mM $[Ru(bpy)_3]^{2+}$ and 50 mM TEA donor (no CO_2 added) with a 405 nm (170 mW) light pulse of 7.2 s duration, growth of $[Co^{I}\mathbf{N_4H}(MeCN)]^+$ was observed under loss of $[Co^{II}\mathbf{N_4H}(MeCN)]^{2+}$ according to first-order kinetics (the mechanism of visible-light-induced electron transfer from sensitizer $[Ru(bpy)_3]^{2+}$ or $Ir(ppy)_3$ to catalyst is described in Figures S3 and S4). A series of spectral traces and the kinetic behavior of representative bands are shown in Figure 7A, traces (a), and Figure 7B, respectively. The assignment of the photolysis product can directly be discerned from comparison with the spectrum of as-synthesized $[Co^{I}\mathbf{N_4H}(MeCN)]^+$ reproduced in Figure 7A, trace (b). While as-synthesized $[Co^{I}\mathbf{N_4H}(MeCN)]^+$ is stable for hours in wet acetonitrile solution, $[Co^{I}\mathbf{N_4H}(MeCN)]^+$ formed by visible-light-sensitized reduction spontaneously decreased in the dark on the tens of seconds time scale under regeneration of Co^{II} catalyst complex as indicated by growth at 1278 cm^{-1} (Figure 7A, traces (c), with kinetics shown in Figure S5A). The reaction is attributed to the formation of acidic $N(CH_2CH_3)_3^+$ radical cation upon photosensitized generation of the reduced sensitizer $[Ru(bpy)_3]^+$ (Figure S3). As has been reported previously, $[Co^{I}\mathbf{N_4H}]^+$ in acetonitrile solution exposed to strong acid evolves H_2 under regeneration of Co^{II} catalyst on the time scale of seconds.[15] In addition to the Co^I macrocycle bands, growth of absorption occurs at 1725 cm^{-1} originating from $CH_3CH{=}O$ co-product of TEA oxidation. Acetaldehyde is an established product of the oxidized/deprotonated TEA donor radical in reaction with H_2O,[41]

$$N(CH_2CH_3)_3 + H_2O + 2[Co^{II}\mathbf{N_4H}]^{2+} \rightarrow HN(CH_2CH_3)_2 + 2[Co^{III}\mathbf{N_4H}]^{3+}-H^- + CH_3CH{=}O \quad (1)$$

When photosensitizing the $[Co^{II}\mathbf{N_4H}(MeCN)]^{2+}$ catalyst with the $[Ru(bpy)_3]^{2+}$−TEA system in CO_2-saturated wet CD_3CN solution, a markedly different IR spectrum emerges. As shown in Figure 8a, growth during the initial 3 s of photolysis is at 1324, 1347, 1364, 1435, and >1575 cm^{-1} (the latter overlaps with decreasing bicarbonate bands) characteristic of $[Co^{I}\mathbf{N_4H}]^+-CO_2$ as can be seen by comparison with an authentic spectrum of the complex (Figure 8b). Growth of a broad absorption at 1522 cm^{-1} (^{13}C counterpart at 1499 cm^{-1}), which shows different kinetics than all other increasing bands, is attributed to the formation of some carbamate adduct with the amine group in agreement with the characteristic IR frequency of the CNH bending more around 1500 cm^{-1} and its modest ^{13}C isotope shift.[42,43] Consumption of $[Co^{II}\mathbf{N_4H}]^{2+}-HCO_3^-$ is most clearly seen by decrease of the intense bands at 1278, 1640, and 1674 cm^{-1} (the latter preventing observation of IR growth in the region 1580−1700 cm^{-1} region). The result was confirmed by an experiments with $^{13}CO_2$, which gave the corresponding spectrum of $[Co^{I}\mathbf{N_4H}]^+-^{13}CO_2$ (Figure S6). In the later part of the light pulse between 3 and 7.2 s, growth is dominated by bands at 1310 and 1398 cm^{-1}, which are the two most intense absorptions of $[Co^{I}\mathbf{N_4H}(MeCN)]^+$. The induction period of these features is clearly evident from the kinetic curves shown in Figure 9. Monitoring of the subsequent dark period shows that the $[Co^{I}\mathbf{N_4H}]^+-CO_2$ complex is stable while $[Co^{I}\mathbf{N_4H}(MeCN)]^+$ is depleted by reaction with protons, as expected (Figure 8c and Figure S5B). We conclude that driving the $Co^{II}\mathbf{N_4H}(MeCN)]^{2+}$ catalyst for CO_2 reduction with $[Ru(bpy)_3]^{2+}$ photosensitizer generates the $[Co^{I}\mathbf{N_4H}]^+-CO_2$ complex with complete selectivity at the onset of reaction (Figure 10), followed by conversion to $[Co^{I}\mathbf{N_4H}(MeCN)]^+$ under continued illumination. While the $[Co^{I}\mathbf{N_4H}]^+-CO_2$ complex is stable in the dark, its conversion to $[Co^{I}\mathbf{N_4H}(MeCN)]^+$ under illumination points to dissociation of the initially formed $[Co^{I}\mathbf{N_4H}]^+-CO_2$ by interaction with photogenerated $[Ru(bpy)_3]^+$ and TEA radical cation species. This side reaction is a phenomenon originating from the choice of the photosensitization system and of no relevance to the CO_2 reduction catalysis of interest. It is important to note that

DOI: 10.1021/jacs.6b05248
J. Am. Chem. Soc. 2016, 138, 9959−9967

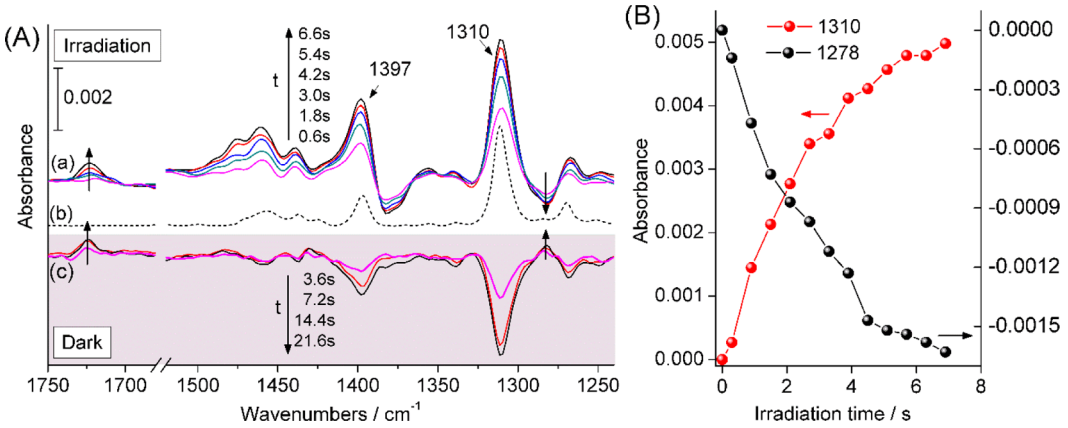

Figure 7. $[Ru(bpy)_3]^{2+}$ visible-light-sensitized reduction of $[Co^{II}N_4H(MeCN)]^{2+}$ in solution containing CD_3CN (0.1 M H_2O), $[Ru(bpy)_3]^{2+}$ (1 mM), $[Co^{II}N_4H(MeCN)]^{2+}$ (3 mM) and TEA (50 mM). (A) (a) FT-IR difference spectra during 7.2 s photolysis, (b) authentic spectrum of $[Co^{I}N_4H(MeCN)]^{+}$, and (c) evolution of spectra during subsequent dark period of 22.8 s. (B) Kinetics of $[Co^{I}N_4H(MeCN)]^{+}$ increase (1310 cm^{-1}) and $[Co^{II}N_4H(MeCN)]^{2+}$ consumption (1278 cm^{-1}) during irradiation.

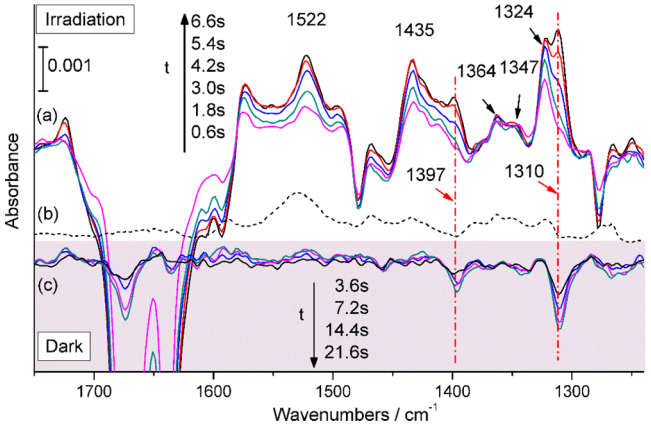

Figure 8. $[Ru(bpy)_3]^{2+}$ visible-light-sensitized reduction of $[Co^{II}N_4H(MeCN)]^{2+}$ in CO_2-saturated solution containing CD_3CN (0.1 M H_2O), $[Ru(bpy)_3{}^{2+}]$ (1 mM), $[Co^{II}N_4H(MeCN)]^{2+}$ (3 mM) and TEA (50 mM): (a) FT-IR difference spectra during 7.2 s photolysis, (b) authentic spectrum of $[Co^{I}N_4H]^{+}-CO_2$, and (c) evolution of spectra during subsequent dark period of 22.8 s.

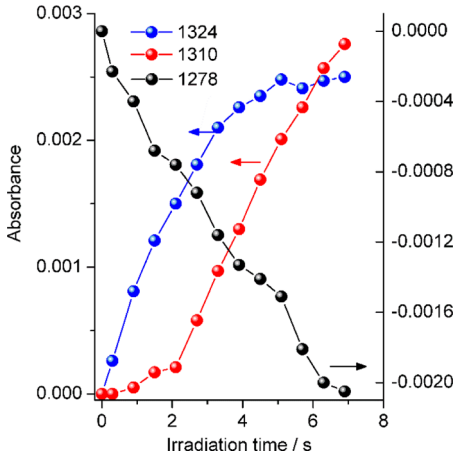

Figure 9. Kinetics of $[Co^{I}N_4H]^{+}-CO_2$ growth (1324 cm^{-1}), $[CoN_4H(MeCN)]^{+}$ increase (1310 cm^{-1}), and $[Co^{II}N_4H(MeCN)]^{2+}$ consumption (1278 cm^{-1}) during irradiation.

the observed stability of the $[Co^{I}N_4H]^{+}-CO_2$ complex in the dark after the end of the photosensitization pulse (Figure 8c)

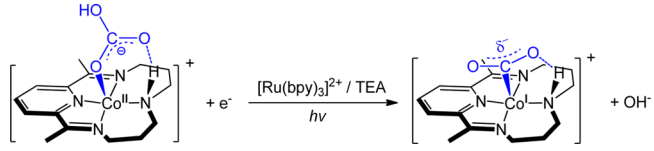

Figure 10. Visible-light-sensitized one-electron reduction of $[Co^{II}N_4H]^{2+}$ bicarbonate complex to $[Co^{I}N_4H]^{+}$ complex with CO_2.

rules out any interaction of the reduced $[Co^{I}N_4H]^{+}-CO_2$ complex with transient TEA radical;[19,44] the latter reacts with H_2O to yield $CH_3C{=}O$ instead according to the process described in Figure S3.

3.3. CO_2 Reduction with Ir(ppy)$_3$ Sensitizer. Photosensitization of $[Co^{II}N_4H(MeCN)]^{2+}$ catalyst (3 mM) in CD_3CN solution (0.1 M H_2O) using Ir(ppy)$_3$ sensitizer (0.2 M, maximum concentration in wet acetonitrile) and TEA donor (50 mM) with 405 nm light (170 mW) showed growth of $[Co^{I}N_4H(MeCN)]^{+}$ under depletion of $[Co^{II}N_4H(MeCN)]^{2+}$ as in the case of the experiment with $[Ru(bpy)_3]^{2+}$ sensitizer (Figure S7, upper part). The $[Co^{I}N_4H(MeCN)]^{+}$ complex reacted spontaneously with protons as shown in the bottom part of Figure S7. Hence, the process induced by the reduction of the catalyst in the absence of CO_2 is independent of the photosensitizer employed.

When photosensitization of $[Co^{II}N_4H(MeCN)]^{2+}$ was conducted in CO_2-saturated wet CD_3CN solution with Ir(ppy)$_3$ sensitizer for the duration of 7.2 s, growth of an IR spectrum was observed with most but not all bands in agreement with those of the $[Co^{I}N_4H]^{+}-CO_2$ complex. Specifically, increasing absorptions at 1324, 1364, 1435, and >1575 cm^{-1} are the same as those of the $[Co^{I}N_4H]^{+}-CO_2$ complex observed in the $[Ru(bpy)_3]^{2+}$-sensitized experiments, and also show first-order growth kinetics (Figure 11a). However, the profile of the symmetric carboxylate stretch absorption in the 1340−1360 cm^{-1} region is distinctly different, as will be described in detail below. Furthermore, in contrast to the $[Ru(bpy)_3]^{2+}$-sensitized experiment, negligible growth of $[Co^{I}N_4H(MeCN)]^{+}$ caused by a secondary photolysis process was detected; i.e., sensitization by Ir(ppy)$_3$ does not result in significant dissociation of the $[Co^{I}N_4H]^{+}-CO_2$ complex. Most importantly, the intermediate produced by Ir(ppy)$_3$ photosensitization decreased spontaneously on the tens of seconds time scale under regeneration of the starting $[Co^{II}N_4H]^{2+}-$

DOI: 10.1021/jacs.6b05248
J. Am. Chem. Soc. 2016, 138, 9959−9967

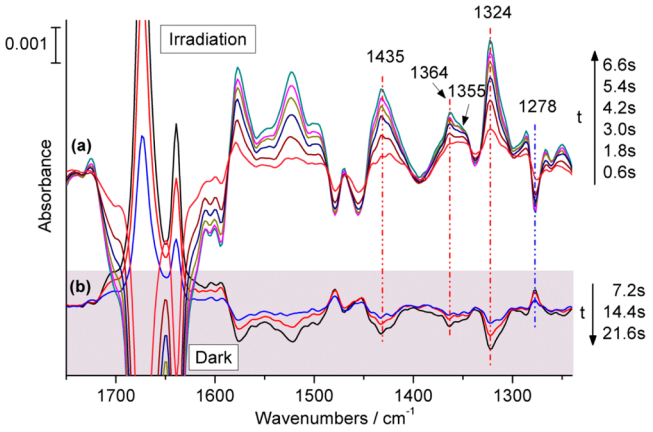

Figure 11. $Ir(ppy)_3$ visible-light-sensitized reduction of $[Co^{II}\mathbf{N_4H}(MeCN)]^{2+}$ in CO_2-saturated solution containing CD_3CN (0.1 M H_2O), $Ir(ppy)_3$ (0.2 mM), $[Co^{II}\mathbf{N_4H}(MeCN)]^{2+}$ (3 mM), and TEA (50 mM): (a) FT-IR difference spectra during 7.2 s photolysis and (b) evolution of spectra during subsequent dark period of 22.8 s.

HCO_3^- complex as indicated by growth of the peaks at 1278, 1640, and 1674 cm^{-1} (Figure 11b; ^{13}C counterparts at 1590 and 1628 cm^{-1}, as shown in Figure S8). Therefore, despite similarities of parts of the spectra, the transient intermediate observed with the $Ir(ppy)_3$ sensitizer is not the $[Co^{I}\mathbf{N_4H}]^{+}$–$CO_2$ species, as the latter was found to be stable after termination of the photosensitization pulse.

A detailed study of the spectral changes in the 1300–1400 cm^{-1} region of $Ir(ppy)_3$-sensitized experiments with $^{12}CO_2$ and $^{13}CO_2$ provided the critical insights into the structure of the new intermediate. The upper part of Figure 12 compares time slices in the 1450–1250 cm^{-1} region during photosensitization recorded at 0.6, 3.0, and 6.6 s for (A) $[Ru(bpy)_3]^{2+}/^{12}CO_2$, (B) $Ir(ppy)_3/^{12}CO_2$, and (C) $Ir(ppy)_3/^{13}CO_2$ systems, with each trace showing the result of spectral deconvolution. The $[Ru(bpy)_3]^{2+}$ and the $Ir(ppy)_3$-sensitized experiments of Figure 12A and 12B were conducted with $^{12}CO_2$ and exhibit first-order growth of the 1324, 1364, and 1435 cm^{-1} bands mentioned above. Figure 13A shows the growth kinetics of the 1324 cm^{-1} absorption for the $Ir(ppy)_3$ run (for the $[Ru(bpy)_3]^{2+}$ experiment, the 1310 cm^{-1} band of $[Co^{I}\mathbf{N_4H}(MeCN)]^{+}$ due to dissociation of $[Co^{I}\mathbf{N_4H}]^{+}$–$CO_2$ is observed to grow in with an induction period). A distinct feature of the $Ir(ppy)_3$-sensitized experiment is that the 1347 cm^{-1} band of the carboxylate ligand of the one-electron-reduced $[Co^{I}\mathbf{N_4H}]^{+}$–$CO_2$ complex decreases after initial sharp rise and then remains unchanged, as can be seen from the red spectral component of Figure 12B, traces (a)–(c), and Figure 13A. By contrast, in the $[Ru(bpy)_3]^{2+}$ run the 1347 cm^{-1} mode of $[Co^{I}\mathbf{N_4H}]^{+}$–$CO_2$ increases with first-order kinetics during the photolysis pulse (Figure 12A, red-colored component of traces (a)–(c)). In the $Ir(ppy)_3$ run, a new band at 1355 cm^{-1} grows in with an induction period, as can be seen by the blue component in Figure 12B, traces (a)–(c), and the kinetic curve in Figure 13A. This band is absent in Ru-sensitized experiments. When conducting the $Ir(ppy)_3$-sensitized experiment with $^{13}CO_2$, the 1355 cm^{-1} band does not appear while a new band is seen to grow in at 1310 cm^{-1} with the same kinetic behavior as the 1355 cm^{-1} absorption (Figure 12C, traces (a)–(c), and Figure S8). The isotope shift confirms assignment of the 1355 cm^{-1} peak to the symmetric stretch of carboxylate. The kinetic behavior of the 1347 and 1355 cm^{-1} bands of the carboxylate ligand indicates that the same $[Co^{I}\mathbf{N_4H}]^{+}$–$CO_2$ one-electron-reduced intermediate is produced in the $Ir(ppy)_3$ and $[Ru(bpy)_3]^{2+}$-sensitized experiment, but followed by a second reduction step that yields a new intermediate when using the Ir sensitizer. The added electron of the new intermediate essentially resides on the CO_2 ligand because the IR bands of the macrocycle are the same within our spectral resolution (4 cm^{-1}) as those for the one-electron-reduced intermediate. The blue shift of the symmetric carboxylate stretch mode is consistent with the increased negative charge on the CO_2

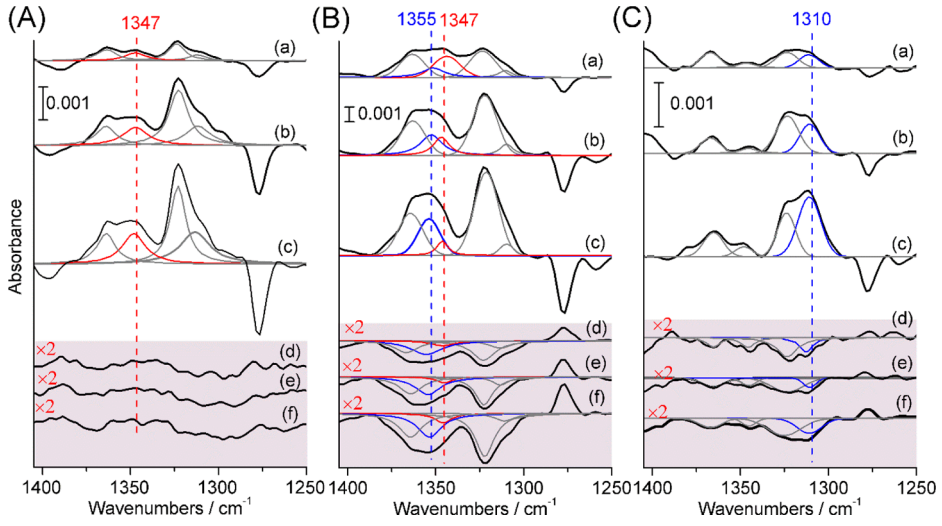

Figure 12. Visible-light-sensitized reduction of $[Co^{II}\mathbf{N_4H}(MeCN)]^{2+}$ in CO_2-saturated solution containing CD_3CN (1 M H_2O), 3 mM $[Co^{II}\mathbf{N_4H}(MeCN)]^{2+}$, and 50 mM TEA. (A) $[Ru(bpy)_3]^{2+}$ (1 mM), $^{12}CO_2$. (B) $Ir(ppy)_3$ (0.2 mM), $^{12}CO_2$. (C) $Ir(ppy)_3$ (0.2 mM), $^{13}CO_2$. Spectra (a)–(c) were recorded during illumination at 0.6, 3.0, and 6.6 s (spectra taken before illumination as background). Spectra (d)–(f) were collected during subsequent dark period at 7.2, 14.4, and 21.6 s after the end of illumination (spectrum at 0.3 s after illumination taken as background). Spectral deconvolution was conducted with OPUS software. (When increasing the water concentration from 0.1 to 1 M, the cycling of $[Co^{I}\mathbf{N_4H}(MeCN)]^{+}$ became much faster, so the accumulation of $[Co^{I}\mathbf{N_4H}(MeCN)]^{+}$ during photolysis with $[Ru(bpy)_3]^{2+}$ as sensitizer is much less than that with 0.1 M water.).

DOI: 10.1021/jacs.6b05248
J. Am. Chem. Soc. 2016, 138, 9959–9967

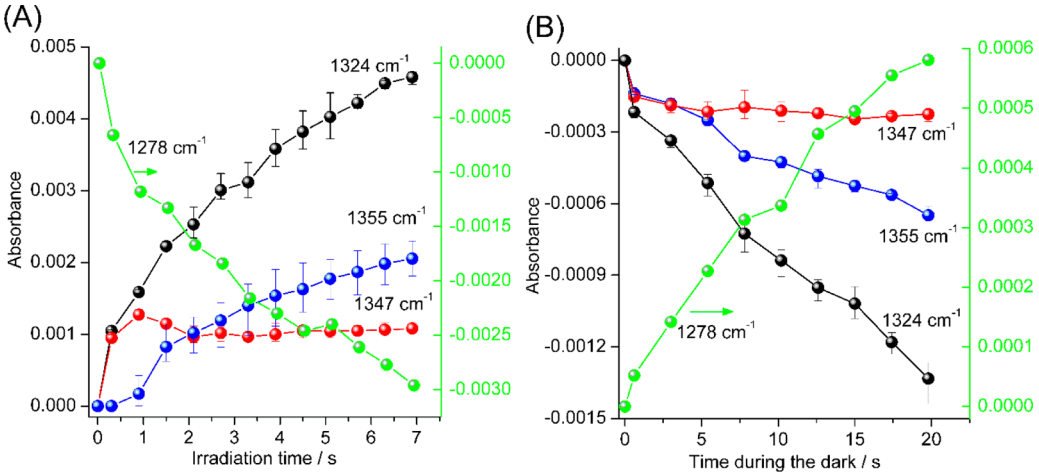

Figure 13. Kinetic behavior of $[Co^{I}N_4H]^{+}-CO_2$ (1347 cm^{-1}) and $[Co^{I}N_4H]^{+}-CO_2^{-}$ (1355 cm^{-1}) intermediates upon photosensitization with $Ir(ppy)_3$. (A) During 405 nm photosensitization period of 7.2 s. (B) During subsequent 20 s dark period. The 1324 cm^{-1} band of the macrocycle is common to both intermediates. The 1278 cm^{-1} trace shows the depletion (panel A) and regeneration (panel B) of the $[Co^{II}N_4H]^{2+}$ catalyst.

ligand.[45] We conclude that the two-electron-reduced intermediate is a $[Co^{I}N_4H]^{+}-CO_2^{-}$ complex.

In the subsequent dark period following $Ir(ppy)_3$ photosensitization for 7.2 s, the 1355 cm^{-1} band together with 1324, 1364, 1435 cm^{-1} decrease under regeneration of $[Co^{II}N_4H]^{2+}-HCO_3^{-}$ as indicated by growth at 1278, 1640, and 1674 cm^{-1}. Figure 11b shows consecutive spectral traces at 7.2, 14.4, and 21.6 s after the end of the photolysis pulse, while traces (d)−(f) of Figure 12B present on an expanded scale the behavior of the individual spectral components. The stretch mode of the CO_2^{-} ligand at 1355 cm^{-1} (blue-colored band) decreases along with the macrocycle absorptions at 1324, 1364, 1435 cm^{-1}. For $Ir(ppy)_3$-sensitized reduction of $^{13}CO_2$ in shown in Figure 12C, traces (d)−(f), the decrease of the corresponding isotopically shifted CO_2 mode is observed at 1310 cm^{-1}. Over an identical 22 s dark period following 7.2 s photosensitized reduction of $^{13}CO_2$ using $Ir(ppy)_3$, growth of free ^{13}CO product in solution is observed at 2080 cm^{-1}, as shown in Figure 14. Because of the weak IR band of dissolved CO in wet acetonitrile, chloroform was added to the CH_3CN (1.0 M H_2O) solution for this experiment which allowed to increase the concentration of $Ir(ppy)_3$ to 1 mM and enhance the solubility of CO. It is important to note that during the dark period, any effect of the decomposition products of the oxidized TEA donor on reactivity is absent because these are known to be limited to the sub-millisecond time range.[44] We conclude that photosensitization with $Ir(ppy)_3$ results in the reduction of $[Co^{II}N_4H]^{2+}-HCO_3^{-}$ complex to $[Co^{I}N_4H]^{+}-CO_2$ and subsequently to a two-electron-reduced catalyst intermediate with $[Co^{I}N_4H]^{+}-CO_2^{-}$ structure. This catalytic intermediate spontaneously eliminates CO under regeneration of the catalyst $[Co^{II}N_4H]^{2+}-HCO_3^{-}$ complex on the time scale of several seconds at room temperature, as summarized in Figure 15.

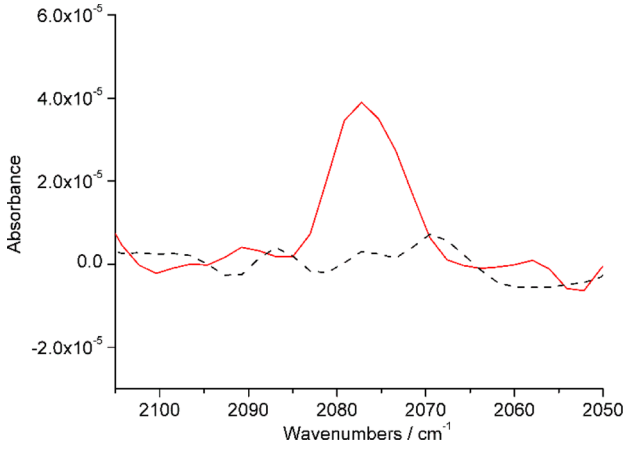

Figure 14. Growth of ^{13}CO in solution during 20 s dark period following $Ir(ppy)_3$-photosensitized reduction of $^{13}CO_2$ in wet acetonitrile-chloroform mixture ($CHCl_3$:CH_3CN 1:1 v/v, 0.1 M H_2O) for 7.2 s (red trace). Control experiment with $^{12}CO_2$ (black dashed trace).

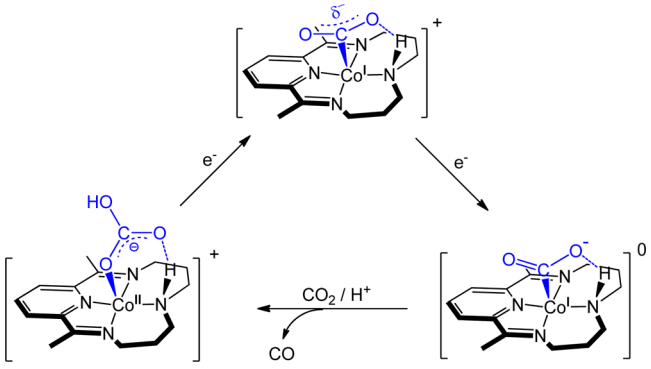

Figure 15. Sequential one- and two-electron intermediates of CO_2 reduction to CO by $[CoN_4H(MeCN)]^{2+}$ catalyst in wet acetonitrile solution.

4. DISCUSSION

The virtually unchanged IR bands of the macrocycle ligand of the two-electron-reduced $[Co^{I}N_4H]^{+}-CO_2^{-}$ intermediate formed upon delivery of the second electron to the one-electron-reduced $[Co^{I}N_4H]^{+}-CO_2$ complex reveal that the electronic structure of the macrocycle of the two intermediates closely resemble one another. The significant blue shift of the symmetric CO_2 stretch of the $[Co^{I}N_4H]^{+}-CO_2^{-}$ intermediate indicates that the added electron mainly resides on the CO_2 ligand rather than on the macrocycle. This finding is in

DOI: 10.1021/jacs.6b05248
J. Am. Chem. Soc. 2016, 138, 9959−9967

remarkable agreement with the previously published DFT electronic structure calculations, which predicted a stable adduct of two-electron-reduced Co tetracycle and CO_2 in acetonitrile.[32] As shown in Figure 8 of ref 32, the computed structure features a carboxylate moiety interacting with the Co center through carbon and has substantial density of the second added electron on the Co^I-CO_2 bond as well as the oxygen atoms of CO_2. The stability of the $[Co^I\mathbf{N_4H}]^+-CO_2^-$ intermediate relative to the dissociated form in acetonitrile was calculated as 7.6 kcal mol^{-1}, for which hydrogen bonding between CO_2^- and the N−H group of the macrocycle plays a significant role. The spontaneous dissociation of the CO_2 ligand of the transient $[Co^I\mathbf{N_4H}]^+-CO_2^-$ intermediate to CO under regeneration of the $[Co^{II}\mathbf{N_4H}]^+$ resting state observed here by FT-IR spectroscopy on the time scale of seconds (Figures 11−14) indicates a barrier of just a few kcal mol^{-1} for this rate-limiting step. The C−O bond dissociation of the CO_2^- ligand might be aided by transfer of the departing O to a free CO_2, resulting in the formation of the bicarbonate ligand of the emerging $[Co^{II}\mathbf{N_4H}]^+$ catalyst complex. While speculative, such a direct role of dissolved carbon dioxide as a Lewis acid in assisting CO bond dissociation has been invoked in a previous IR spectro-electrochemical study of CO_2 reduction by a Ni cyclam catalyst.[46]

In contrast to the two-electron-reduced intermediate, the complex of the one-electron-reduced $[Co^I\mathbf{N_4H}]^+$ macrocycle with CO_2 is substantially less stable (by 10 kcal mol^{-1}) according to the DFT study.[32] Nevertheless, we find distinct IR signature of the interaction of CO_2 with the one-electron-reduced catalyst. Specifically, the symmetric and asymmetric IR stretch modes of the CO_2 ligand of the 5-coordinate $[Co^I\mathbf{N_4H}]^+-CO_2$ complex (Figures 4, 5, and 8) indicate a significantly bent carboxylate structure. Furthermore, this fifth ligand markedly influences the structure of the macrocycle as evidenced by substantial differences of the IR macrocycle modes of the $[Co^I\mathbf{N_4H}]^+-CO_2$ and the $[Co^I\mathbf{N_4H}(MeCN)]^+$ complexes. The structure of the latter was previously established by single crystal XRD.[29] Weak H bonding between the N−H group of the macrocycle and O of the CO_2 ligand of $[Co^I\mathbf{N_4H}]^+-CO_2$ predicted by the DFT calculation is borne out by the 21 cm^{-1} red shift of the N−H stretch mode seen in the FT-IR spectra of Figure 5. The formation of the $[Co^I\mathbf{N_4H}]^+-CO_2$ intermediate is completely selective both when using the Ru or Ir sensitizer, an important finding regarding the quest for steering the competition between CO_2 reduction and proton reduction toward CO_2 activation (the observed dissociation of the complex by a secondary photolysis process to generate $[Co^I\mathbf{N_4H}(MeCN)]^+$ when using Ru sensitizer is a phenomenon caused by the chosen photosensitization method, and is not an intrinsic property of the $[Co^I\mathbf{N_4H}]^+-CO_2$ intermediate. As the Ir-sensitized experiment shows, transfer of a second electron with sufficient reducing power to the $[Co^I\mathbf{N_4H}]^+-CO_2$ intermediate eliminates the formation of $[Co^I\mathbf{N_4H}(MeCN)]^+$).

A key finding of the present study is that the one-electron-reduced $[Co^I\mathbf{N_4H}]^+-CO_2$ intermediate is sufficiently stable in wet acetonitrile at room temperature to directly capture a second electron. Because the ensuing $[Co^I\mathbf{N_4H}]^+-CO_2^-$ intermediate spontaneously dissociates to CO, the selectivity of molecular catalysts toward CO_2 reduction can be enhanced by maximizing the fraction of one-electron catalyst intermediates forming an adduct with CO_2.

5. CONCLUSIONS

In summary, FT-IR monitoring of the reduction of CO_2 by the Co tetracycle catalyst $[Co^{II}\mathbf{N_4H}(MeCN)]^{2+}$ in wet acetonitrile solution driven by $Ir(ppy)_3$ visible light sensitizer allowed the detection and identification of a two-electron-reduced intermediate $[Co^I\mathbf{N_4H}]-CO_2^-$(complex of the Co tetracycle with CO_2^-). This intermediate spontaneously dissociates in a rate-limiting step to CO on the time scale of seconds at room temperature under regeneration of the catalyst in the resting state. The macrocycle IR modes indicate that the electronic structure of the two-electron intermediate is close to that of the one-electron-reduced complex $[Co^I\mathbf{N_4H}]^+-CO_2$ with a Co^I center, neutral $\mathbf{N_4H}$ ligand, and a second electron residing mainly on the carboxylate moiety. This finding is in good agreement with a previous DFT electronic structure calculation which predicted that the two-electron-reduced intermediate is a stable adduct of Co^I tetracycle and CO_2, with substantial density of the second electron on the carboxylate ligand.[32]

An important result regarding design features for steering molecular catalysts from proton toward CO_2 reduction is that the second electron delivered to the $[Co^I\mathbf{N_4H}]^+-CO_2$ complex (one-electron-reduced catalyst) selectively generates an even stronger $[Co^I\mathbf{N_4H}]^+-CO_2^-$ complex that spontaneously dissociates to free CO under regeneration of the catalyst. This suggests that the ability to form an adduct with CO_2 upon transfer of the first electron plays a critical role. This adduct needs to have sufficient lifetime to receive a second electron while still intact. There is likely an optimal stability range for the one-electron $[Co^I\mathbf{N_4H}]^+-CO_2$ adduct; too strong interaction might lead to an unreactive complex upon reduction by the second electron, while too little interaction would result in insufficient lifetime (concentration) of the $[Co^I\mathbf{N_4H}]^+-CO_2$ adduct for capturing a second electron.

■ ASSOCIATED CONTENT

Supporting Information

The Supporting Information is available free of charge on the ACS Publications website at DOI: 10.1021/jacs.6b05248.

Figures S1−S8, showing rapid-scan FT-IR spectra of reactions, spectra of reagents, kinetic data, and photosensitization mechanism (PDF)

■ AUTHOR INFORMATION

Corresponding Author

*hmfrei@lbl.gov

Notes

The authors declare no competing financial interest.

■ ACKNOWLEDGMENTS

This work was supported by the Joint Center for Artificial Photosynthesis, a DOE Energy Innovation Hub, supported through the Office of Science of the U.S. Department of Energy under Award No. DE-SC0004993, and by the Director, Office of Science, Office of Basic Energy Sciences, Division of Chemical, Geological and Biosciences of the U.S. Department of Energy under Contract No. DE-AC02-05CH11231. H.F. thanks Profs. Jonas Peters, Caltech, and Martin Head-Gordon, UC Berkeley and LBNL, for insightful discussions.

■ REFERENCES

(1) Fisher, B.; Eisenberg, R. *J. Am. Chem. Soc.* **1980**, *102*, 7361−7363.

DOI: 10.1021/jacs.6b05248
J. Am. Chem. Soc. 2016, 138, 9959−9967

(2) Schneider, J.; Jia, H. F.; Kobiro, K.; Cabelli, D. E.; Muckerman, J. T.; Fujita, E. *Energy Environ. Sci.* **2012**, *5*, 9502−9510.
(3) Schneider, J.; Jia, H.; Muckerman, J. T.; Fujita, E. *Chem. Soc. Rev.* **2012**, *41*, 2036−2051.
(4) Kumar, B.; Llorente, M.; Froehlich, J.; Dang, T.; Sathrum, A.; Kubiak, C. P. *Annu. Rev. Phys. Chem.* **2012**, *63*, 541−569.
(5) Thoi, V. S.; Kornienko, N.; Margarit, C. G.; Yang, P. D.; Chang, C. J. *J. Am. Chem. Soc.* **2013**, *135*, 14413−14424.
(6) Tinnemans, A. H. A.; Koster, T. P. M.; Thewissen, D. H. M. W.; Mackor, A. *Recl. Trav. Chim. Pays-Bas* **1984**, *103*, 288−295.
(7) Artero, V.; Chavarot-Kerlidou, M.; Fontecave, M. *Angew. Chem., Int. Ed.* **2011**, *50*, 7238−7266.
(8) Dempsey, J. L.; Brunschwig, B. S.; Winkler, J. R.; Gray, H. B. *Acc. Chem. Res.* **2009**, *42*, 1995−2004.
(9) Han, Z.; Eisenberg, R. *Acc. Chem. Res.* **2014**, *47*, 2537−2544.
(10) Artero, V.; Fontecave, M. *Chem. Soc. Rev.* **2013**, *42*, 2338−2356.
(11) Rakowski Dubois, M.; Dubois, D. L. *Acc. Chem. Res.* **2009**, *42*, 1974−1982.
(12) Zee, D.; Chantarojsiri, T.; Long, J.; Chang, C. J. *Acc. Chem. Res.* **2015**, *48*, 2027−2036.
(13) Kaeffer, N.; Chavarot-Kerlidou, M.; Artero, V. *Acc. Chem. Res.* **2015**, *48*, 1286−1295.
(14) Wang, M.; Chen, L.; Sun, L. *Energy Environ. Sci.* **2012**, *5*, 6763−6768.
(15) Varma, S.; Castillo, C. E.; Stoll, T.; Fortage, J.; Blackman, A. G.; Molton, F.; Deronzier, A.; Collomb, M. N. *Phys. Chem. Chem. Phys.* **2013**, *15*, 17544−17552.
(16) McCrory, C. C. L.; Uyeda, C.; Peters, J. C. *J. Am. Chem. Soc.* **2012**, *134*, 3164−3170.
(17) Leung, C. F.; Chen, Y. Z.; Yu, H. Q.; Yiu, S. M.; Ko, C. C.; Lau, T. C. *Int. J. Hydrogen Energy* **2011**, *36*, 11640−11645.
(18) Ogata, T.; Yanagida, S.; Brunschwig, B. S.; Fujita, E. *J. Am. Chem. Soc.* **1995**, *117*, 6708−6716.
(19) Grodkowski, J.; Dhanasekaran, T.; Neta, P.; Hambright, P.; Brunschwig, B. S.; Shinozaki, K.; Fujita, E. *J. Phys. Chem. A* **2000**, *104*, 11332−11339.
(20) Grodkowski, J.; Neta, P.; Fujita, E.; Mahammed, A.; Simkhovich, L.; Gross, Z. *J. Phys. Chem. A* **2002**, *106*, 4772−4778.
(21) Sampson, M. D.; Froehlich, J. D.; Smieja, J. M.; Benson, E. E.; Sharp, I. D.; Kubiak, C. P. *Energy Environ. Sci.* **2013**, *6*, 3748−3755.
(22) Smieja, J. M.; Kubiak, C. P. *Inorg. Chem.* **2010**, *49*, 9283−9289.
(23) Machan, C. W.; Sampson, M. D.; Chabolla, S. A.; Dang, T.; Kubiak, C. P. *Organometallics* **2014**, *33*, 4550−4559.
(24) Kou, Y.; Nabetani, Y.; Masui, D.; Shimada, T.; Takagi, S.; Tachibana, H.; Inoue, H. *J. Am. Chem. Soc.* **2014**, *136*, 6021−6030.
(25) Hayashi, Y.; Kita, S.; Brunschwig, B. S.; Fujita, E. *J. Am. Chem. Soc.* **2003**, *125*, 11976−11987.
(26) Agarwal, J.; Fujita, E.; Schaefer, H. F.; Muckerman, J. T. *J. Am. Chem. Soc.* **2012**, *134*, 5180−5186.
(27) Grills, D. C.; Farrington, J. A.; Layne, B. H.; Lymar, S. V.; Mello, B. A.; Preses, J. M.; Wishart, J. F. *J. Am. Chem. Soc.* **2014**, *136*, 5563−5566.
(28) Bourrez, M.; Orio, M.; Molton, F.; Vezin, H.; Duboc, C.; Deronzier, A.; Chardon-Noblat, S. *Angew. Chem., Int. Ed.* **2014**, *53*, 240−243.
(29) Lacy, D. C.; McCrory, C. C. L.; Peters, J. C. *Inorg. Chem.* **2014**, *53*, 4980−4988.
(30) McKone, J. R.; Marinescu, S. C.; Brunschwig, B. S.; Winkler, J. R.; Gray, H. B. *Chem. Sci.* **2014**, *5*, 865−878.
(31) Eckenhoff, W. T.; McNamara, W. R.; Du, P.; Eisenberg, R. *Biochim. Biophys. Acta, Bioenerg.* **2013**, *1827*, 958−973.
(32) Zhang, M.; El-Roz, M.; Frei, H.; Mendoza-Cortes, J. L.; Head-Gordon, M.; Lacy, D. C.; Peters, J. C. *J. Phys. Chem. C* **2015**, *119*, 4645−4654.
(33) Hartman, K. O.; Hisatsune, I. C. *J. Chem. Phys.* **1966**, *44*, 1913−1918.
(34) Baylis, B. K. W.; Bailar, J. C. *Inorg. Chem.* **1970**, *9*, 641.
(35) Su, C.; Suarez, D. L. *Clays Clay Miner.* **1997**, *45*, 814.
(36) Lefevre, G. *Adv. Colloid Interface Sci.* **2004**, *107*, 109−123.
(37) David, S. J.; Ault, B. S. *J. Phys. Chem.* **1982**, *86*, 4618−4622.
(38) Fujita, E.; Furenlid, L. R.; Renner, M. W. *J. Am. Chem. Soc.* **1997**, *119*, 4549−4550.
(39) Fujita, E.; Creutz, C.; Sutin, N.; Brunschwig, B. S. *Inorg. Chem.* **1993**, *32*, 2657−2662.
(40) Fujita, E. *Coord. Chem. Rev.* **1999**, *185*−*186*, 373−384.
(41) De La Fuente, J. R.; Canete, A.; Saitz, C.; Jullian, C. *J. Phys. Chem. A* **2002**, *106*, 7113−7120.
(42) Colthup, N. B.; Daly, L. H.; Wiberley, S. E. *Introduction to IR and Raman Spectroscopy*, 3rd ed.; Academic Press: Boston, 1990; p323.
(43) Danon, A.; Stair, P. C.; Weitz, E. *J. Phys. Chem. C* **2011**, *115*, 11540−11549.
(44) Rodenberg, A.; Orazietti, M.; Probst, B.; Bachmann, C.; Alberto, R.; Baldridge, K. K.; Hamm, P. *Inorg. Chem.* **2015**, *54*, 646−657.
(45) Busca, G.; Lorenzelli, V. *Mater. Chem.* **1982**, *7*, 89−126.
(46) Froehlich, J. D.; Kubiak, C. P. *J. Am. Chem. Soc.* **2015**, *137*, 3565−3573.

DOI: 10.1021/jacs.6b05248
J. Am. Chem. Soc. 2016, 138, 9959−9967